J Appl Electrochem (2013) 43:245–252
DOI 10.1007/s10800-012-0510-5

ORIGINAL PAPER

# Improved electrochemical performances of sulfur-microporous carbon composite electrode for Li/S battery

**Sun-Hwa Yeon · Kyu-Nam Jung · Sukeun Yoon · Kyoung-Hee Shin · Chang-Soo Jin · Youngchul Kim**

Received: 21 August 2012 / Accepted: 26 November 2012 / Published online: 9 December 2012


**Abstract** A sulfur-microporous (S-MIP) carbon composite was prepared for use as a cathode for rechargeable Li/S batteries. Two sulfur-embedded methods, S-impregnation (IS) and S-liquefied pore filling (LS), were applied for the preparation of the S-MIP carbon composites. The pristine elemental S of the polycrystalline $\alpha$-$S_8$ undergoes a structural change to an amorphous-S (a-S) structure in the S-MIP carbon composite created by the IS method. During sulfur loading of 40–50 wt %, the S-MIP carbon composite created by the IS method showed a BET SSA value of around 500 $m^2$ $g^{-1}$ and a pore volume of 0.2 $cm^3$ $g^{-1}$. However, after the LS process was applied to the S-MIP carbon composite, at 160 °C and 10 h, the a-S structure in the S-MIP carbon composite became recrystalline $\alpha$-$S_8$. Little remained of the porosity in the S-MIP carbon composite prepared by the LS method due to the large portion of the S crystalline phase. The best discharge capacity was obtained with an S-MIP carbon composite created by the IS method, with the result of 680 mA h $g^{-1}$ after 50 cycles at 0.1 °C, i.e., ~47 % higher than that by the LS method.

**Keywords** Lithium–sulfur · Rechargeable battery · Microporous carbon · Structural change

**Electronic supplementary material** The online version of this article (doi:10.1007/s10800-012-0510-5) contains supplementary material, which is available to authorized users.

S.-H. Yeon (✉) · K.-N. Jung · S. Yoon · K.-H. Shin · C.-S. Jin
Energy Storage Group, Korea Institute of Energy Research, 152, Gajeong-ro, Yuseong, Daejeon 305-343, Republic of Korea
e-mail: ys93@kier.re.kr

Y. Kim
Agency for Defense Development, Yuseong, P. O. Box 35-4, Daejeon 305-600, Republic of Korea

## 1 Introduction

An increasing number of electric or plug-in hybrid vehicles, portable electronic devices, and power tool technologies require significant improvements of rechargeable battery technologies to achieve higher energy capacities. Elemental sulfur (S) is very attractive as a cathode material for high specific energy rechargeable Li batteries because a battery based on the Li/S combination would yield the highest theoretic capacity of about 1,675 mA h $g^{-1}$ with a theoretic specific energy of 2,600 Wh $kg^{-1}$. This supports the electrochemical redox reaction $16Li + S_8 \leftrightarrow 8Li_2S$ [1–3]. S has advantages as it is inexpensive, abundant, and non-toxic. Sulfur shows an intrinsic protection mechanism from an overcharged state when operated in batteries, while providing a safe wide temperature range of operation as well as the possibility of long-term cycling. Therefore, S has been a promising cathode material for high specific energy Li/S batteries [4]. However, although this system has been attracting attention for more than two decades, it has not been commercialized due to several remaining unsolved problems, such as the inherent poor electrical conductivity of S ($5 \times 10^{-30}$ S $cm^{-1}$ at 25 °C), the shuttle effect of higher-order polysulfides during charging, and the rapid decrease in the capacity during cycling (0.1–0.4 % per cycle) [2]. Shuttling is a cyclic process that occurs between lower-order and higher-order forms of polysulfide during the operation of a battery [1, 5–7]. Long-chain Li polysulfides, ($Li_2Sn$, $2 < n < 8$), created at the cathode, can dissolve into the electrolyte and transfer to the anode, where they react with the Li electrode in order to generate lower-order polysulfides, resulting in an undesired parasitic reaction [7]. The shuttle effect leads to the random precipitation of $Li_2S_2$ and $Li_2S$ on the positive electrode, which dramatically changes the electrode morphology and

thus results in fast capacity fading. In order to improve the cycle life of Li/S batteries, preventing polysulfide dissolution is one of the key issues.

To improve the Li/S performance and cycle life, several methodologies have been presented. The major one is to physically restrain polysulfide dissolution using barrier materials, which include carbon coatings on sulfur, high surface area carbon additives [8, 9], conducting polymers [10, 11], and polymeric electrolytes [12]. Out of these physical restraint methodologies, the most attractive method is the incorporation of S into porous host (mostly carbon) structures that contain polysulfides due to the high capacity offered by the porosity [13–16]. Porous materials have attracted attention in many practical fields related to chemical, environmental and energy, electronics, and biotechnological applications due to their regular pore structure [17–20]. Many forms of carbon and metal–organic framework compounds (MOF), optimized for extremely high specific surface areas and specific micropore volumes [21, 22], are candidates for achieving the micropore criteria. Recently discovered MOFs provide exceptionally high surface areas ($\sim$3,000 $m^2$ $g^{-1}$). Also, carbide-derived carbons (CDCs) are well known to possess tunable pore structures and narrow pore size distributions in the 0.5–2 nm range, which can be formed through the selective etching of crystalline metal carbides. This chemical etching method generates microporosity which affords high specific surface areas, large pore volumes, and large adsorption capacities. It also allows pore size matching to different molecules [23, 24]. On the other hand, in practical applications including catalysis and adsorbents more than 2 nm in molecular size, these applications are often limited by their small pore size. The mesoporous materials make a larger contribution because the range of their pore sizes offers the accommodation of complex chemicals, molecular complexes, and even bimolecular materials. The functionalities of large complex molecules, which can depend on their flexible conformational changes, motion, or diffusion, are more likely to be preserved within mesopores.

Recently, electrode composites for Li/S batteries have been prepared using a matrix of mesoporous materials due to their favorable pore dimensions and large pore volumes for capturing the byproduct polysulfide [25]. However, studies of microporous carbon structures with a high BET SSA in the range of 2,000–3,000 $m^2$ $g^{-1}$ [26, 27] have not focused on the carbon/S composite due to smaller pore size (average pore size, <1.0 nm) than the molecular size of sulfur molecule ($S_8$) or polysulfide. In previous studies of microporous materials, it was only reported that its combination of meso/micropores makes it a good electrode material for Li/S batteries due to the favorable adsorption of polysulfides and the easy mass transport of $Li^+$ during the battery operation [14, 28]. Nonetheless, there have been few studies of the S/C structure in a microporous carbon matrix or from a morphology point of view for the operation of Li/S batteries.

In this study, we prepared a S-microporous (S-MIP) carbon composite using two impregnation methods, S-impregnation (IS) and S-liquefied pore filling (LS), and investigated its structural changes and their improved effects on the electrochemical performance in a Li–S rechargeable battery.

## 2 Experimental

### 2.1 Preparation of cathode

The microporous activated carbon (MSP-20, $\sim$2,400 $m^2$ $g^{-1}$) was obtained from Kansai Coke and Chemicals Co., Ltd. This microporous carbon was denoted as MIP carbon. The elemental S powder was purchased from SigmaAldrich (100 mesh particle size, reagent grade). The two S loading processes are as follows. (I) S-impregnation (IS) method: Active S powder is dissolved in $CS_2$ solution to be 10 wt% S solution. The 10 wt% S solution is added to a microporous carbon matrix (MSP-20) that contains the same pore volume as the volume of solution. This solution is added dropwise to the carbon matrix during intensive mixing. At the completion of the addition, the matrix is slightly wet. Immediately afterward, the resulting precursor is dried for 16 h at 60–70 °C. We denoted the prepared S-MIP carbon composite prepared by the IS process as IS20, IS30, IS40, and IS50, according to loaded S, which was 20, 30, 40, and 50 wt%, respectively. (II) S-liquefied pore filling (LS) method: The LS is carried out by heating the above S-MIP carbon composite prepared by the IS process in the quartz tube under an Ar flow at 160 °C for 10 h. In most of the previous studies using porous carbon matrix for cathode material of Li/S battery, this LS process has mainly been by heating the S-carbon mixture at around 160 °C and 10 h under the protection of inert gas. The reason was that elemental $S_8$ became liquid and had the lowest viscosity at 160 °C. Therefore, the liquid S could be infused into the host structure [29]. S-MIP carbon composite prepared by the IS process shows S loss of about 7 wt% after the LS process. We denoted the S-MIP carbon composite by the LS process as LS25, LS50, and LS68, based on the amount of loaded sulfur, which was 25, 50, and 68 wt%, respectively. Cathode electrode material was prepared by adding Super-P (5–10 %) as a conductive additive and polyvinyl fluoride (PVDF, 5–10 %) as a binder in all cases.

### 2.2 Electrochemical evaluation

To evaluate the electrochemical performance of the S-MIP carbon composite prepared by the two processes, 2032-type

coin cells (MTI) were fabricated. The prepared sample was pressed onto an aluminum substrate as the working electrode, including binder and conductive additives. Li was used as the counter electrode. The separator used was CelgardR 3501. Two kinds of electrolytes were used: (i) 0.2 M of $LiNO_3$ + 1 M of Li $CF_3SO_3$ in EG DME/dioxolane = 50:50 (v/v), denoted as Li $CF_3SO_3$; (ii) 0.2 M of $LiNO_3$ + 1 M of Li TFSI in 1,3-dioxolane and 1,2-dimethoxyethane (volume ratio 1:1), denoted as LiTFSI. The specific capacities were calculated based on only the sulfur mass.

## 3 Results and discussion

Evidence of S containment and the identification of an imbedded sulfur structure within the S-MIP carbon composite were provided by TEM images and XRD. Under normal conditions, S atoms form cyclic octatomic molecules with the chemical formula $S_8$. $S_8$ is highly polymorphic and can form different crystal structures (orthorhombic α-$S_8$ of Fddd and monoclinic β-$S_8$ and γ-$S_8$ of $P_2/c$) [30]. The α-$S_8$ is the most stable form in normal conditions [31, 32]. Figures 1a, b, c, d show a pristine S powder, MIP carbon, and S-MIP carbon prepared by the IS and LS processes. In Fig. 1a, the pristine S powder shows crystalline structures with d-spacings (2 2 2) of α-$S_8$, i.e., around 0.3 nm. Amorphous carbon was observed at the MIP carbon possessing shorter and less structured fringes. The inset of Fig. 1b shows the EDS result of the MIP carbon, indicating only the C peak (the Cu peak from the TEM grid). For IS40 prepared by the IS method in Fig. 1c, the crystalline α-$S_8$, which was shown in pristine S powder (Fig. 1a), was not found in this sample. From this result, it is estimated that the amorphous sulfur (a-S) phase can be mixed with an amorphous carbon (a-C) phase homogeneously, which makes it very difficult to distinguish a-S from a-C (See Figure S1). However, in the LS50 sample created by the LS process shown in Fig. 1d, crystalline S was clearly detected in various regions. It was usually sandwiched between amorphous carbon layers. In this case, the resulting crystalline phases of the LS composite are considered as stemming from the recrystallization of amorphous S phase from IS composite, as the LS composite was obtained in the condition of 160 °C and 10 h after the IS process (See Figure S1). The S structure by X-ray diffraction can be cross-checked with the results of the TEM images. The S powder indicates orthorhombic α-$S_8$ with the space group Fddd, as shown in Fig. 1e. The IS40 and IS26 samples showed one broad peak from a-S in the 2θ range of 20–25°, in which there were no S crystalline peaks due to the a-S structure. On the other hand, crystalline α-$S_8$ peaks were noted in the LS50 and LS68 samples, indicating the high α-$S_8$ intensity in LS68 as compared to that in LS50. These XRD results are in good agreement with the TEM results shown in Fig. 1d.

TGA and DTG were performed in an air environment to determine the S content and the mechanism of S incorporation in the MIP carbons. Figures 2a, b show the TGA and DTG curves, respectively, of the LS68, IS40, and IS20 composite samples along with pristine S powder and melted S powder prepared at 160 °C for 10 h. As shown in Fig. 2, the pristine S powder was burned completely at around 350 °C and the pure MIP carbon started to be oxidized at 450 °C, as indicated by the ~100 % weight loss at around 600 °C. Sulfur exists in different allotropic forms, as explained in XRD analysis, which differ in their physical and chemical properties. The principal allotropes are orthorhombic α-$S_8$, monoclinic β-$S_8$, and polymeric $S_w$ [31, 32]. The α-$S_8$ and β-$S_8$ allotropes are both crystalline materials consisting of $S_8$ rings, while $S_w$ consists of chains of up to 106 sulfur atoms. Upon rapid cooling from the melt above 160 °C, plastic sulfur is obtained, which is a mixture of polymeric sulfur and non-crystalline $S_8$. In pristine S powder (Fig. 2), two obvious peaks were observed in the DTG at 244 °C and 320–360 °C, which may correspond to the decomposition temperatures of crystalline α-$S_8$ and the mixture of polymeric sulfur and non-crystalline $S_8$. In the DTG curves of IS40, one peak was observed at ~310 °C, which corresponds to the value between the two DTG peaks at ~244 °C and 320–360 °C of the pristine S. This may result from the S absorption strength in the carbon structures as possible S–C bonding of the type, occurring in MIP carbon-S composites. On the other hand, in LS68, two peaks were observed at ~244 and ~300 °C with small fluctuations. The first peak shown at ~244 °C for LS68 is well matched with the first peak (crystalline α-$S_8$ phase) in pristine S powder. The second peak shown at ~300 °C of the LS68 is close to the peak shown in the DTG curves of IS40 and IS26 related to the possible S–C bonding phase. It is expected that crystalline and non-crystalline phases coexist in the LS68 composite.

A Raman spectroscopy analysis of the pristine S, pure MIP carbon, IS26, and LS50 samples (Fig. 3) was performed at different laser powers of 0.6 mW (Fig. 3a, b) and 0.1 mW (Fig. 3c, d) in the full (100–4,000 $cm^{-1}$) and 150–1,000 $cm^{-1}$ range. The Raman spectra were normalized to the intensity of the G-band at 1,582 $cm^{-1}$. Graphitic materials were characterized by bands labeled as D (~1,356 $cm^{-1}$, disorder mode), G (~1,579 $cm^{-1}$, in-plane vibrational mode), and 2D (~2,706 $cm^{-1}$, second-order mode). The MIP carbon exhibited the broad D band typical of amorphous disordered carbon. After the impregnation of sulfur, typical D and G peaks of carbon remained in the IS26 and LS50 samples. In the pristine sulfur powder, as verified by the XRD and TEM results, strong Raman modes of sulfur, $\nu_1$, $\nu_2$, and $\nu_8$, were

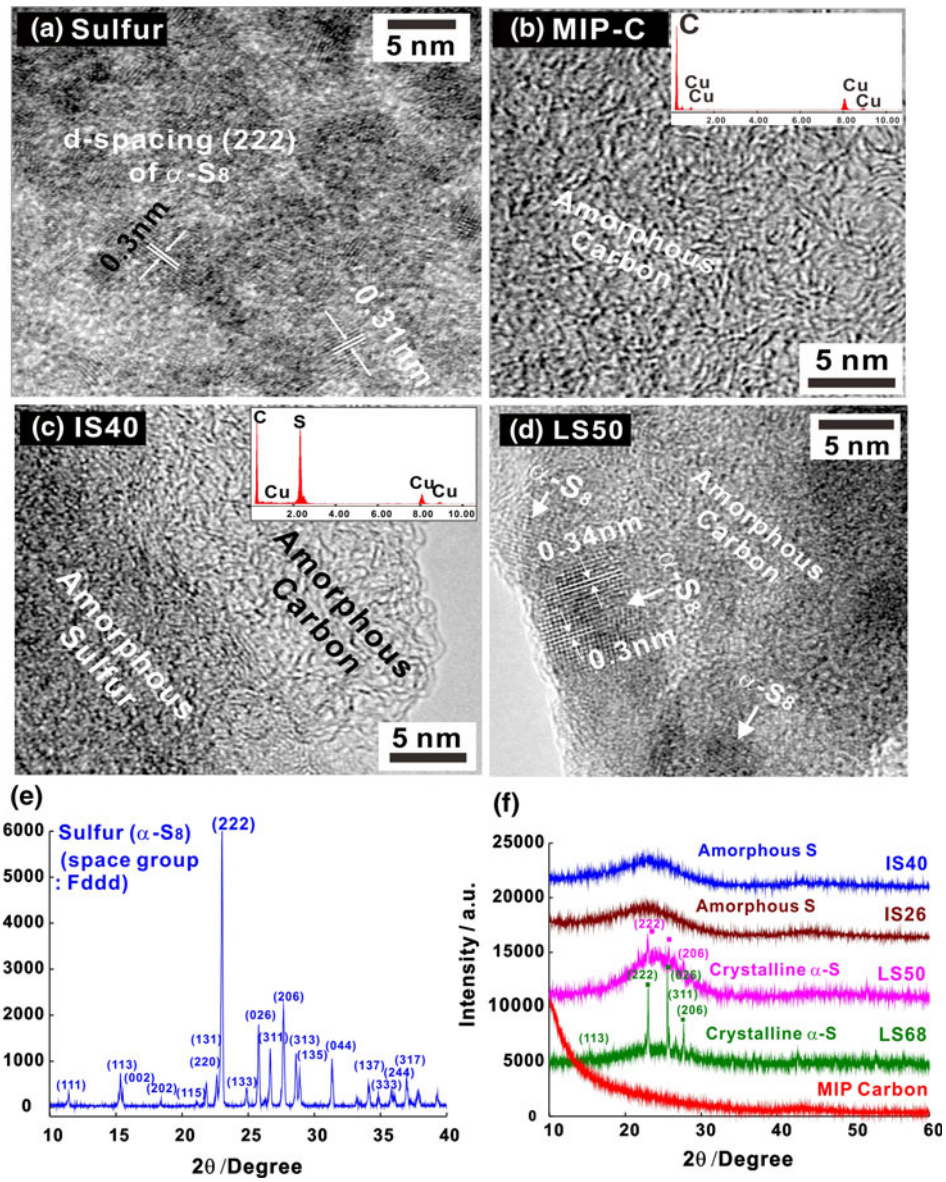


**Fig. 1** TEM images (**a**–**d**) and X-ray diffraction (**e**–**f**) of pristine S powder, MIP carbon, and S-MIP carbon composites. Pristine S powder (**a**). MIP carbon with inset of EDS (**b**). S-MIP carbon composite prepared by IS process with inset of EDS (**c**). S-MIP carbon composite prepared by LS process (**d**). X-ray diffraction of pristine S powder (**e**), MIP carbon and S-MIS carbon composites by IS and LS process (**f**)

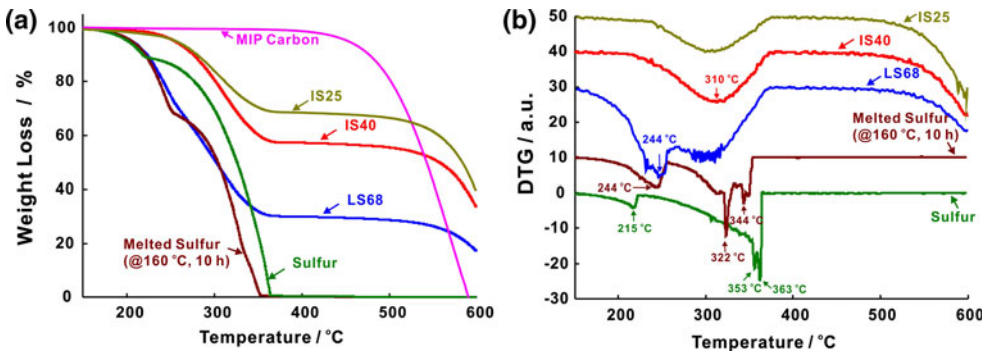


**Fig. 2** Thermogravimetric analysis of TGA (**a**) and DTG (**b**) curves of S, S melted at 160 °C for 10 h, IS26, IS40, LS68, and MIP carbon

observed at 155, 220, and 476 $cm^{-1}$, respectively, at a laser power of 0.6 mW, which is in agreement with the previously reported values of polycrystalline S [33]. Weak Raman modes were observed at 189, 250, and 440 $cm^{-1}$, as shown in Fig. 3b. After the LS method on the MIP carbon of the LS50 sample, three strong Raman peaks of sulfur, $\nu_1$, $\nu_2$, and $\nu_8$, were retained, while weak Raman modes were detected. On the other hand, the Raman mode was not detected in IS26 prepared by the IS method due to structural changes in the polycrystalline S to an amorphous state after impregnation. In order to

prevent damage of the sulfur structure by the Raman laser, a low laser power, 0.1 mW, was used, as shown in Fig. 3c, d. While the Raman mode was still not detected in the IS26 sample, a strong Raman mode was clearly shown in the LS50 sample as shown in Fig. 3d. In order to confirm the surface functionality, the Fourier transform infrared (FTIR) spectra of bare sulfur, IS26, and LS68 composites were assessed in the 400–4,000 $cm^{-1}$ wave number range (Fig. S2). While the various peaks shown in IS26 and LS68 are similar to those of bare sulfur, the distinct peak in the range of 1,050–1,200 $cm^{-1}$, which is expected to be the characteristic C=S peak, was detected only in the carbon–sulfur composite.

Figure 4 shows the $N_2$ adsorption isotherms and the estimated PSDs of the MIP carbon, LS26, and LS40. The SSA and PSD of the composites were analyzed through $N_2$ adsorption/desorption measurements at 77 K. Table 1 shows the porosity characteristics of MIP carbon, IS26, IS40, LS50, LS68, and pristine S from the $N_2$ isotherms. The MIP carbon showed an isotherm of typical type I, as shown in Fig. 4a. After sulfur loading, the $N_2$ sorption isotherms of both IS26 and IS40 still maintained type I only after reducing the amount of the total adsorbed $N_2$. The MIP carbon showed a high BET SSA, 2,418 $m^2\ g^{-1}$, with a total pore volume of 1.05 $cm^3\ g^{-1}$. After S loading, the remaining portions of the micropore volume at IS26 and IS40 were 85 and 80 %, respectively, of their total pore volume. At sulfur loading levels of 40–50 %, the MIP carbon composite created by the IS method showed a BET SSA of approximately 500 $m^2\ g^{-1}$ and a pore volume of 0.2 $cm^3\ g^{-1}$, which could provide room or reaction sites for polysulfide during the operation of a battery. However, for the LS50 and LS68 samples, little remained of the total pore volume due to the large portion of sulfur content with crystalline phase, which can reduce the reaction site for battery operation.

The voltage profiles of the S-MIP carbon composite, IS26, at two electrolytes, in this case $LiCF_3SO_3$ and LiTFSI, are shown in Fig. 5. For IS26 using $LiCF_3SO_3$ in Fig. 5a, the discharge profiles show the typical two-plateau behavior of a S cathode, which correspond to the formation of long-chain polysulfide ($Li_2S_x$, $4 \leq x \leq 8$) at 2.4 V and short-chain polysulfide $Li_2S_2$ and $Li_2S$ at 2.03 V, indicating an elemental $S_8$ reduction to $S_6^{2-}$ and $S_2^{2-}$, respectively. Moreover, the flat second plateau suggests a uniform deposition of $Li_2S$ with few kinetic barriers. Similar results were found when the electrolyte of LiTFSI was used as shown in Fig. 5b. On the other hand, in LS68 which used LiTFSI, only one voltage plateau was noted around 2.4 V, and no further discharge reaction was evident afterward as shown in Fig. 5c. The differences in the response appear to have been strongly related to how thoroughly the S was incorporated into the carbon. C–S bonding and the S structure in carbon can change the equilibrium potential of S–Li reactions and the electrochemical capacity. In the S-MIP carbon composite created by the LS process, it is estimated that the crystalline phase of S influences the Li/S

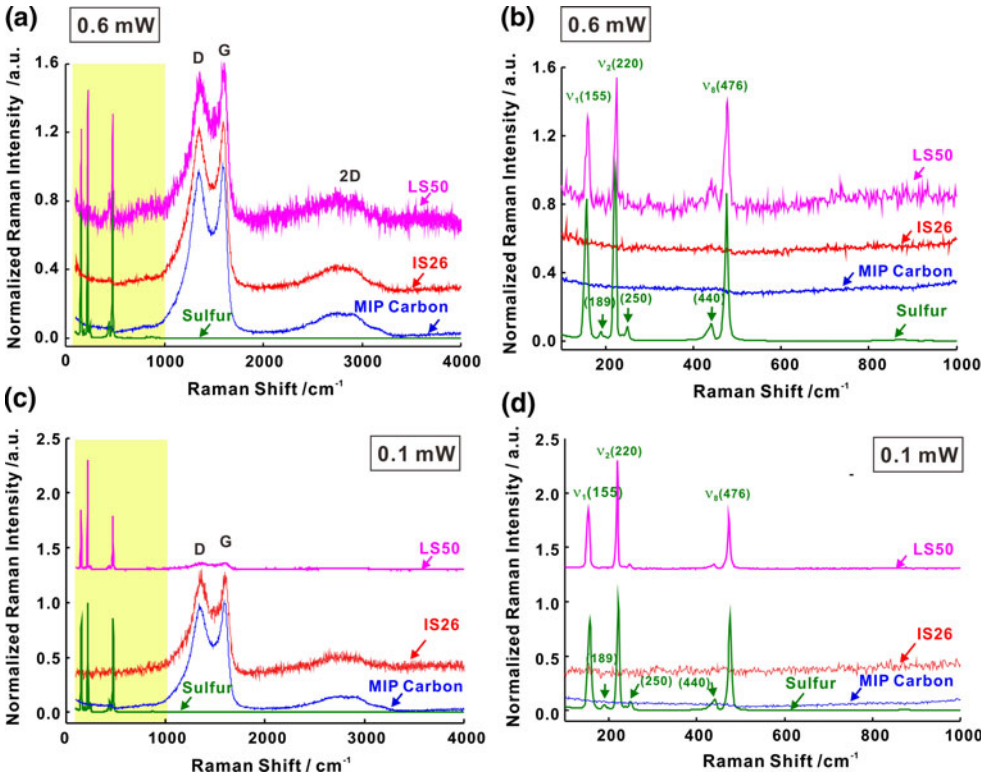


**Fig. 3** Raman spectra of pristine S, IS26, LS50, and pure MIP carbons at 0.6 mW (**a**, **b**) and 0.1 mW (**c**, **d**) in 100–4,000 $cm^{-1}$ range (**a**, **c**) and 150–1,000 $cm^{-1}$ range (**b**, **d**)

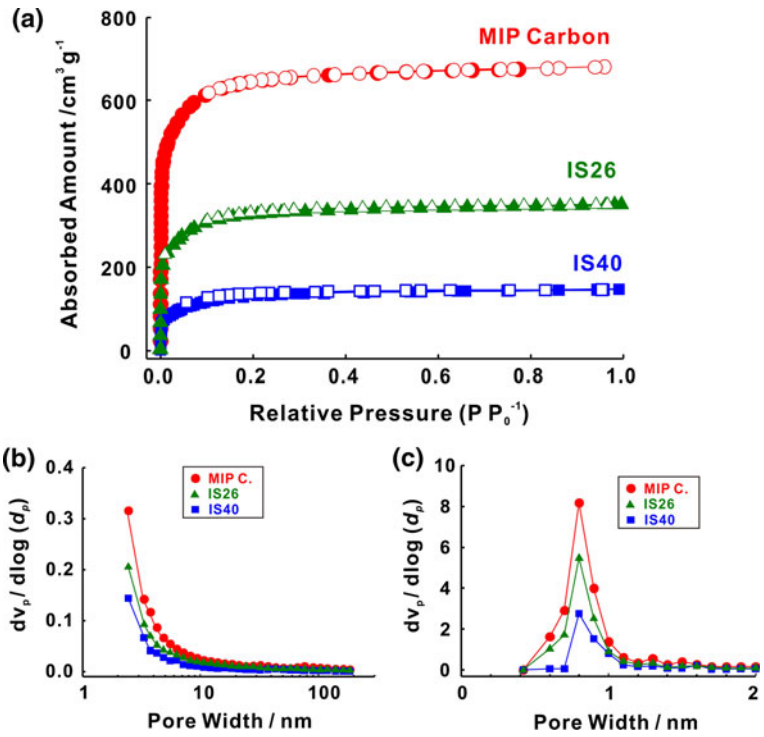


**Fig. 4** $N_2$ adsorption/desorption characterization of S-MIP carbon composite: **a** isotherms at 77 K for MIP carbon, LS26, and LS40; **b** pore size distribution calculated by BJH method using the adsorption branch of isotherm; **c** pore size distribution calculated by MP method. Solid symbols correspond to sorption and empty symbols to desorption of nitrogen

**Table 1** S contents (%), S loading (mg) per electrode ($cm^2$), and porosity characteristics of MIP carbon, IS26, IS40, LS25, LS50, LS68, and pristine S

| Materials | Sulfur content (wt%) | Sulfur loading of electrode (mg-S $cm^{-2}$) | BET SSA ($m^2$ $g^{-1}$) | Total pore volume ($cm^3$ $g^{-1}$) | Mesopore volume by BJH ($cm^3$ $g^{-1}$) | Micropore volume by MP ($cm^3$ $g^{-1}$) |
|---|---|---|---|---|---|---|
| MIP carbon | 0 | 0 | 2418 | 1.06 | 0.13 | 1.09 |
| IS26 | 26 | 1.16 | 1189 | 0.54 | 0.08 | 0.55 |
| IS40 | 40 | 2.02 | 502 | 0.22 | 0.05 | 0.22 |
| LS25 | 25 | 0.89 | 900 | 0.46 | 0.06 | 0.46 |
| LS50 | 50 | 0.845 | 7.08 | – | – | – |
| LS68 | 68 | 3.64 | 0.73 | – | – | – |
| S | 100 | – | 0.082 | – | – | – |

reaction. The low porosity of the LS composite (Table 1) caused by excessive sulfur content along with crystalline S phase may result in a low discharge capacity (Fig. 5c) due to the difficulty in providing the room or reaction sites for polysulfide during operation.

The cyclic performances of the IS26, IS40, LS25, LS50, and LS68 electrodes using two electrolytes are presented in Fig. 6. The sulfur loadings (mg per $cm^2$ electrode) for each electrode are shown in Table 1. In previous research, pristine S showed poor cycling stability with a rapid discharge capacity fading. The discharge capacity decreased from 1,100 mA h $g^{-1}$ at the first cycle to 240 mA h $g^{-1}$ at the 25th cycle [34, 35]. However, an improvement of the capacity performance and the cycling stability was clearly shown with the S-MIP carbon composite. The best discharge capacity and cycle life were obtained with the IS26 composite electrode created by the IS method, which used $LiCF_3SO_4$ and LiTFSI at a sulfur loading of 26 wt%, resulting in 680 mA h $g^{-1}$ after 50 cycles at a 0.1 °C rate. This is ~13.6 and ~6.8 % greater than the results shown in previous studies for S-microporous carbon composites using a carbon matrix of a-MPC (50 mA h $g^{-1}$ at 50 cycle) and WVA-1500 (100 mA h $g^{-1}$ at 50 cycle), respectively [36, 37]. On the other hand, in the LS68 electrode, the electrochemical performance showed a low capacity of ~200 mA h $g^{-1}$ after 50 cycles, which was ~82 % smaller than the MIP carbon composite created by the IS method. In the case of LS50 electrode prepared by the same process, while the electrochemical performance was ~900 mA h $g^{-1}$ in the LITFSI electrolyte from the second

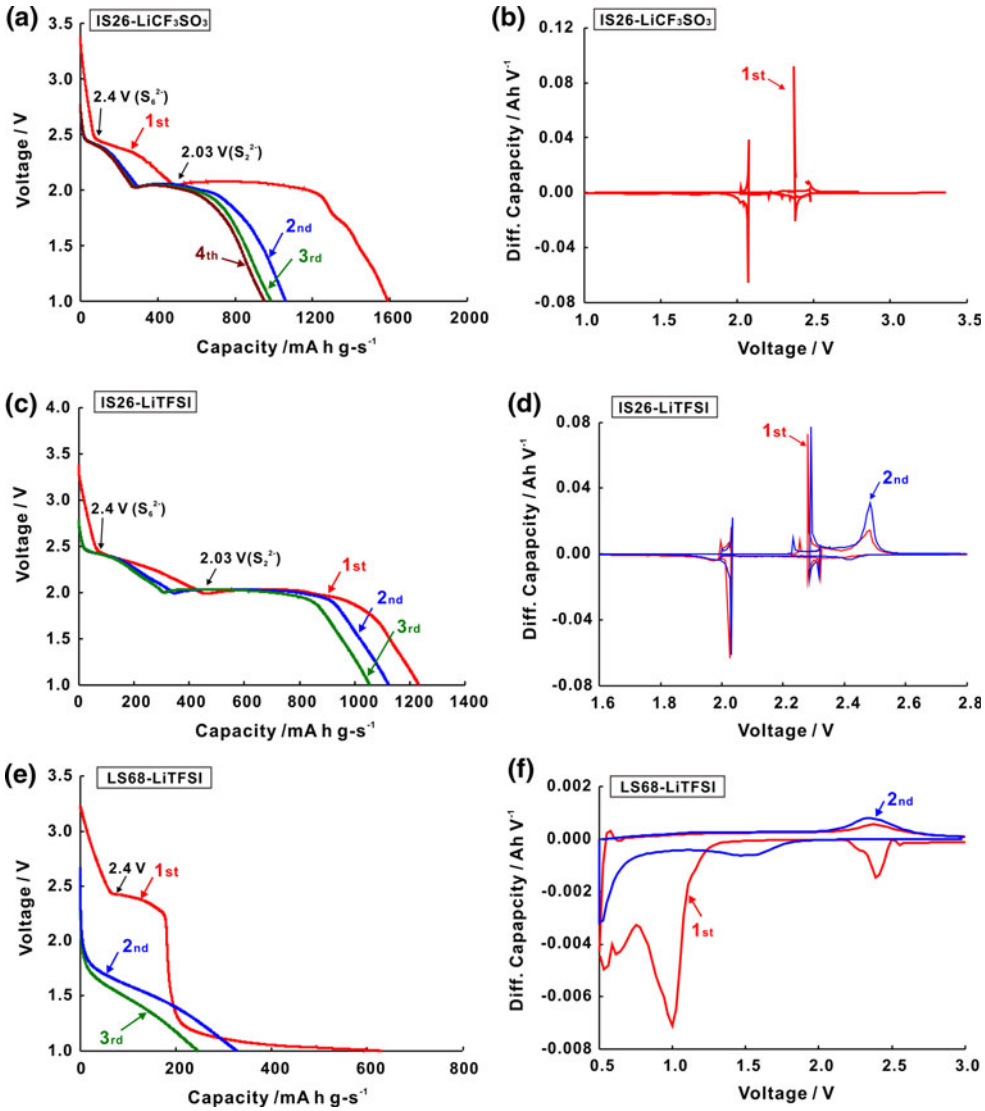


**Fig. 5** Voltage and differential capacity (dqdv) profiles of the electrodes prepared by IS26 (**a**, **b**, **c**, **d**) and LS68 (**e**, **f**) using different electrolytes of $LiCF_3SO_3$ (**a**, **b**), LiTFSI (**c**, **d**, **e**, **f**)

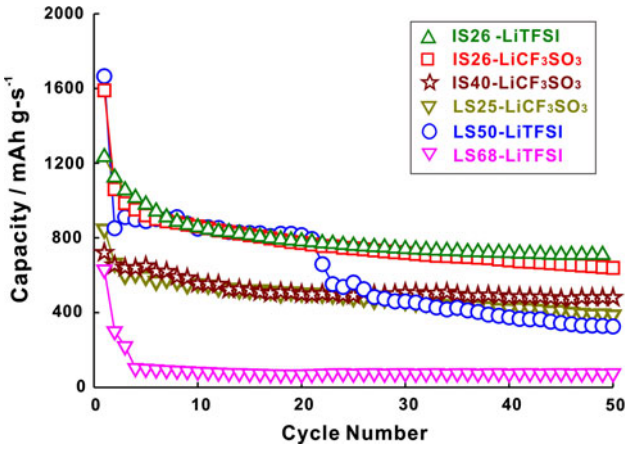


**Fig. 6** Cycle life of various S-MIP carbon composite cathodes according to two electrolytes of $LiCF_3SO_3$ and LiTFSI. All samples were performed at 0.1 °C rate

cycle, it started to decrease rapidly after 20 cycles ($\sim$328 mA h $g^{-1}$ at 50 cycles). In the similar sulfur loading case of IS26 and LS25 using $LiCF_3SO_4$, the IS26 composite (387 mA h $g^{-1}$) showed a result $\sim$1.8 times higher than that of the LS25 composite at 50 cycles.

## 4 Conclusions

In this study, an S-MIP carbon composite was synthesized in a microporous carbon matrix using the IS and LS methods for a Li–S battery. While the S-MIP composite prepared by the LS method possessed an orthorhombic $\alpha$-$S_8$, the MIP carbon created by the IS method showed an amorphous sulfur structure without any crystallite. From the porosity data, at a sulfur loading of 40–50 %, the MIP carbon created by the IS method showed a BET SSA value of around 500 $m^2$ $g^{-1}$ and a pore volume of 0.2 $cm^3$ $g^{-1}$,

which could provide room or reaction sites for polysulfide during operation due to the homogeneous amorphous phases of the MIP carbon and sulfur. However, little remained of the porosity of the MIP carbon created by the LS method due to the large portion of sulfur crystalline phase, resulting in a low discharge capacity. The IS26 electrode could retain a discharge capacity of $\sim$680 mA h $g^{-1}$ after 50 cycles at a 0.1 °C rate when the electrolyte of 1 M LiTFSI was used (1,200 mA h $g^{-1}$ at the first cycle). In the LS68 electrode, the electrochemical performance showed a low capacity of $\sim$200 mA h $g^{-1}$ after 50 cycles, which was $\sim$82 % smaller than the MIP carbon composite created by the IS method. In the similar sulfur loading cases of IS26 and LS25 using $LiCF_3SO_4$, the IS26 composite (387 mA h $g^{-1}$) showed a final result that was $\sim$1.8 times higher than that of the LS25 composite at 50 cycles. The amorphous S structure is important in the sulfur-microporous (S-MIP) carbon composite, which can also explain the increase in the electrochemical performance compared to the crystalline S structure in the LS composite due to the greater porosity in the IS composite. The development of high-capacity Li–S battery can be achieved using a S-microporous (S-MIP) carbon composite.

**Acknowledgments** This work was supported by the Next Generation Military Battery Research Center program of The Defense Acquisition Program Administration and Agency for Defense Development. We acknowledge the KAIST Central Research Instrument Facility for the use of Raman and TEM facilities, the National NanoFab Center for FT-IR facilities, and the KIER R & D Activity Center for SEM and XRD facilities.

## References

1. Ji X, Nazar LF (2010) J Mater Chem 20:9821
2. Jayaprakash N, Shen J, Moganty SS et al (2011) Angew Chem Int Ed 50:5904
3. Ji L, Rao M, Zheng H et al (2011) J Am Chem Soc 133:18522
4. Kolosnitsyn VS, Karaseva EV (2008) Rus J Electrochem 44:506
5. Ji X, Evers S, Black R, Nazar LF (2011) Nat Commun 2:325
6. Barchasz C, Leprêtre J-C, Alloin F, Patoux S (2012) J Power Sources 199:322
7. Barchasz C, Mesguich F, Dijon J et al (2012) J Power Sources 211:19
8. Choi Y-J, Kim K-W, Ahn H-J, Ahn J-H (2008) J Alloy Compd 449:313
9. Zheng W, Liu YW, Hu XG, Zhang CF (2006) Electrochim Acta 51:1330
10. Fanous J, Wegner M, Grimminger J et al (1975) Chem Mater 23:5024
11. Wu F, Chen J, Li L et al (1975) J Phys Chem C 115:24411
12. Hassoun J, Scrosati B (2010) Angew Chem Int Ed 49:2371
13. Wang J, Chew SY, Zhao ZW et al (2008) Carbon 46:229
14. Liang C, Dudney NJ, Howe JY (1975) Chem Mater 21:4724
15. Yeon S-H, Reddington P, Gogotsi Y et al (2010) Carbon 48:201
16. Vakifahmetoglu C, Presser V, Yeon S-H et al (2011) Microporous Mesoporous Mater 144:105
17. Ariga K, Vinu A, Yamauchi Y et al (2012) Bull Chem Soc Jpn 85:1
18. Sumida K, Rogow DL, Mason JA et al (2011) Chem Rev 112:724
19. Xiang Q, Yu J, Jaroniec M (2012) Chem Soc Rev 41:782
20. Dawson R, Cooper AI, Adams DJ (2012) Prog Polym Sci 37:530
21. Ma S, Sun D, Simmons JM et al (2007) J Am Chem Soc 130:1012
22. Wang X-S, Ma S, Rauch K et al (2008) Chem Mater 20:3145
23. Stoeckli F, Centeno TA (2005) Carbon 43:1184
24. Sabo M, Henschel A, Frode H et al (2007) J Mater Chem 17:3827
25. Schuster J, He G, Mandlmeier B et al (2012) Angew Chem Int Ed 51:3591
26. Yeon S-H, Knoke I, Gogotsi Y, Fischer JE (2010) Microporous Mesoporous Mater 131:423
27. Yeon S-H, Osswald S, Gogotsi Y et al (2009) J Power Sources 191:560
28. Liang C, Dudney NJ, Howe JY (2009) Chem Mater 21:4724
29. Guo J, Xu Y, Wang C (2011) Nano Lett 11:4288
30. Vaganova E, Wachtel E, Rozenberg H et al (2004) Chem Mater 16:3976
31. Krossing I (2003) In: Steudel R (ed) Homoatomic sulfur cations: elemental sulfur and sulfur-rich compounds I. Springer, Berlin/Heidelberg
32. Steudel R (2003) In: Steudel R (ed) Liquid sulfur liquid sulfur: elemental sulfur and sulfur-rich compounds I. Springer, Berlin/Heidelberg
33. Aggarwal RL, Farrar LW, Polla DL (2011) J Raman Spectrosc 42:461
34. Liang X, Wen Z, Liu Y et al (2011) J Power Sources 196:3655
35. Liang X, Liu Y, Wen Z et al (2011) J Power Sources 196:6951
36. Wolff MM, Stephens WE (1958) Phys Rev 112:890
37. Sanloup C, Gregoryanz E, Degtyareva O, Hanfland M (2008) Phys Rev Lett 100:075701